

Short-Range Wireless Optical Communication using Pixelated Transmitters and Imaging Receivers

Steve Hranilovic
Department of Electrical and
Computer Engineering
McMaster University

Hamilton, Ontario, L8S 4K1 Canada.
Email: hranilovic@ece.mcmaster.ca

Frank R. Kschischang
Department of Electrical and
Computer Engineering
University of Toronto
Toronto, Ontario, M5S 3G4 Canada.
Email: frank@comm.utoronto.ca

Abstract—Short-range wireless optical channels provide high-data rate indoor links free of spectral licensing issues. In this work, we present a point-to-point, multiple-input/multiple output (MIMO) optical channel, termed the *pixelated wireless optical channel*, which exploits the inherent spatial diversity of the channel to achieve gains in spectral efficiency. Information is conveyed through the transmission of a series of pixelated images to a receiver array. An experimental prototype point-to-point link is constructed using a 512×512 pixel LCD panel and 154×154 pixels of a CCD camera. Based on channel measurements, a channel model amenable to computer simulation is developed. Spatial discrete multitone modulation is proposed for this MIMO wireless optical channel to combat the low pass spatial response of the channel. The capacity of a given channel realization is estimated by way of the water-pouring spectrum. Multi-level coding and multi-stage decoding over the spatial frequency bins is shown to yield spectral efficiencies of approximately 1.7 kbit/s/Hz over a range of 2 m.

I. INTRODUCTION

Wireless optical links transmit information by modulating the instantaneous optical intensity of a light-emitting element and detecting the intensity field using a photodiode receiver. Since the devices can only modulate and detect the optical intensity rather than the amplitude or phase directly, all transmitted signals must be non-negative. Additionally, tight constraints are made on the average optical power (i.e., average amplitude) due to eye and skin safety regulations. Popular configurations for wireless optical channels include (i) point-to-point links in which an optical intensity is transmitted in a directed fashion to the receiver and (ii) diffuse links in which optical radiation is permitted to reflect on surfaces in a room. Both point-to-point and diffuse links are free from multipath fading since the receiver photodiode integrates the optical intensity field over an area of millions of square wavelengths and hence no change in channel response is noted if the receiver is moved on the order of a wavelength [1, 2].

In this work we introduce a point-to-point, multiple-input/multiple-output (MIMO), short-range wireless optical channel, termed the *pixelated wireless optical channel*, which exploits spatial diversity to realize gains in spectral efficiency [3]. The use of multiple optical transmitters has been considered in various contexts: wireless optical links, chip-to-chip interconnect and holographic storage. Multi-element diffuse and

quasi-diffuse wireless optical links using discrete [4, 5] and imaging [6–8] receivers and a variety of combining and coding schemes [9, 10] have been considered to achieve gains in optical power efficiency. However, identical optical signals are transmitted in all spatial directions yielding no improvements in spectral efficiency. Two-dimensional optical chip-to-chip interconnects have been constructed with arrays of vertical cavity surface emitting lasers (VCSELs) and receiver arrays with up to 512 parallel channels each transmitting independent data [11, 12]. Although significant gains in spectral efficiency are available, a common problem in all interconnects of this type is that transmitter and receiver must be tightly aligned to avoid any inter-channel interference [13]. Error control coding has been applied to these links to combat misalignment problems [14–16], however, cross-talk between receive pixels is viewed as noise independent of the received values at each pixel and is not exploited in system design. In holographic storage systems strict spatial alignment is usually present so that each receive element images a single transmit pixel [17, 18]. These “pixel-matched” systems, however, are very sensitive to misalignment errors.

The pixelated optical channel, presented here, differs significantly from previous optical multi-element work. The transmitter consists of a pixelated array of thousands of optical emitters which form a time-varying image on a display screen or on a surface. Images are formed by employing coding over space and time, i.e., *spatio-temporal* coding, to improve the spectral efficiency and reliability of the link. The receiver uses imaging optics and an array of optical detectors to produce a pixelated receive image. This is in contrast to previous multi-element wireless optical links which transmit identical information in all spatial modes, in essence employing an inefficient spatial repetition code. Unlike some chip-to-chip interconnect and holographic systems, strict alignment of the receiver and transmitter are not required so long as the transmitter remains in the field of view of the receiver.

Sec. II describes the pixelated wireless optical channel topology. An experimental prototype link is described and a channel model is derived based on channel measurements. Sec. III describes spatial discrete multitone modulation which is well suited to the pixelated wireless optical channel and

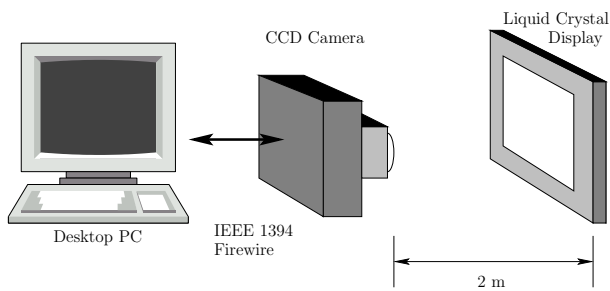


Fig. 1. Diagram of experimental prototype.

estimates the capacity of the channel using a water-pouring argument in spatial frequency domain. A multi-level code and multi-stage decoder is then presented to approach the channel capacity. Finally, Sec. IV presents some concluding remarks and directions for future work.

II. THE PIXELATED WIRELESS OPTICAL CHANNEL

A. Channel Topology

The transmitter is a *spatial light modulator* which produces an output optical intensity spatial distribution which is controlled by optical or electrical addressing [19]. In other words, the transmitter outputs a time-varying optical intensity image which is transmitted in free-space to form an image. This image can be formed on a display as in the case of liquid crystal displays, arrays of light emitting diodes (LEDs) and organic polymer LEDs (OLEDs) or the image can be projected onto a surface (e.g., wall or ceiling) by using an LCD panel or an array of deformable micro-mirror devices (DMD) and the appropriate optics.

The receiver is oriented to capture the transmitted image and produces an output signal representing the spatial distribution of optical power impinging on the device. This device can be thought of as a temporal and spatial optical intensity sampler. Typical two-dimensional examples of such receivers are charge-coupled device (CCD) cameras, CMOS imagers as well as arrays of photodiodes. Appropriate optics are employed to form a focused image on the surface of the detector array.

B. Experimental Prototype

In order to determine the nature of the pixelated optical channel, an experimental point-to-point link, as shown in Fig. 1, was constructed. The transmit array was realized using the LCD panel of a laptop computer [20]. The computer was used to control the LCD panel which measures 12.1" on the diagonal and has 1024×768 pixels at a dot pitch of 0.24 mm. The array of light receivers is implemented by way of a CCD camera [21]. This camera has a resolution of 640×480 pixels of size $10\mu\text{m} \times 10\mu\text{m}$ and can operate at frame rates of 60 frames per second uncompressed video.

The channel is configured so that the optical axes of the transmitter and the receiver are aligned to produce a receive image which is an *orthographic projection* of the transmitted image [22]. As a result, in the absence of any other channel impairments, the received image is a scaled version

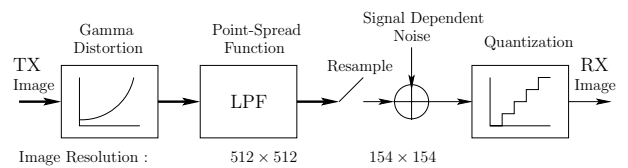


Fig. 2. Block diagram of the channel model for the point-to-point pixelated wireless optical channel.

of the transmitted image. The distance between transmitter and receiver was set at 2 m and no relative motion between ends of the link was present. The lens was manually focused on the LCD panel and the aperture was set to $f/1.6$ for all measurements to minimize detector saturation. Although most commercial short-range wireless optical links operate in the infrared band ($\lambda=850\text{--}950$ nm), this visible band experimental channel illustrates the same design challenges.

C. Channel Model

A channel model is required to allow for the simulation of spatial modulation and coding schemes. The transmitted image is composed of 512×512 pixels of the LCD panel with all other pixels turned off. At the receiver, the corresponding received image is 154×154 pixels in size. Test images were transmitted to characterize the channel impairments and to produce the channel model in Fig. 2.

The point-spread function (PSF) of an optical system is the response of the system to a spatial impulse input and can be used to characterize spatially invariant systems. The PSF was measured at different transmit pixel locations and observed to be low pass in spatial frequency domain. This response is due to the averaging of the CCD array, optical aberrations as well as diffraction effects. The PSF was computed over several transmit pixels and the discrepancy versus the central response was less than 9% in terms of the energy justifying the spatially invariant assumption.

Cathode ray tubes and LCD panels have a non-linear *gamma distortion* between the input level and the optical intensity output [23]. This distortion was measured by displaying a constant frame of differing intensity and averaged over 1000 frames to yield the response

$$J(x, y) = 1.1 \times 10^{-3} I(x, y)^{2.4} + 20.2$$

where $I(x, y)$ is the input image and $J(x, y)$ is the corresponding output.

The noise at each receive pixel is due to background light as well as due to the transmitted signal. The distribution of this noise is typically taken as being Gaussian with variance linearly related to the receive intensity. The variance of the noise was averaged over five locations and 1000 frames. The variance of the noise is least squares fit to a linear model to give $\sigma^2 = \alpha \bar{I} + \beta$, where \bar{I} is the mean received level, $\alpha = 1.9 \times 10^{-2}$ and $\beta = 0.33$ with an R^2 statistic of fit greater than 0.99.

The operation of the CCD imager is represented as a re-sampling of the image to a resolution of 154×154 . This

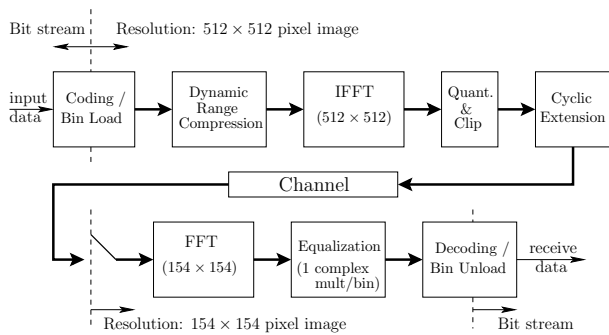


Fig. 3. Block diagram of SDMT system.

re-sampling is done by using bilinear interpolation for non-integer sampling points. Signal-dependent noise is added and the output is quantized to the 8-bit levels available from the camera. A comparison between 100 transmitted binary level images and the output of the channel model gave rise to a 5.4% error in the average energy with respect to the channel measurement. Although not insignificant, the error between the measured data is small enough to suggest that the salient properties of the channel are represented in the model and that the model is appropriate for modem-design purposes.

III. SPATIAL MODULATION AND CODING

In order to realize gains in spectral efficiency, spatio-temporal coding is required. The problem of modem design becomes one of designing a family of time-varying images which are reliably detected by an array of receive elements in the presence of the channel impairments.

A. Spatial Discrete Multitone Modulation

Discrete multitone (DMT) modulation is a popular signalling scheme for frequency selective channels, especially for digital subscriber lines [24–26]. A related scheme, *spatial discrete multitone* (SDMT) modulation is defined here as an extension of the conventional DMT system. The SDMT modulation format forms images by transmitting data in spatial frequency bins subject to a loading algorithm. This technique allows for efficient transmission over the spatial frequency selective pixelated wireless optical channel. Fig. 3 presents a block diagram of the SDMT system.

It is assumed that there is a training period preceding data transmission in which test signals are transmitted to allow the receiver to determine the signal-to-noise ratio in each spatial frequency bin. With this information, the transmitter can compute a power allocation and load the spatial frequency bins appropriately. Sec. III-B illustrates an example of this power allocation for the system under consideration.

After loading the bins, the resulting signal often exhibits a large peak-to-average ratio. This problem is well known in conventional DMT systems [26]. Typically, all the available spatial frequency bins are not allocated with data since the signal-to-noise ratio is too low. A dynamic range-compression algorithm is adapted in a straight forward fashion from the DMT literature which exploits these degrees of freedom to

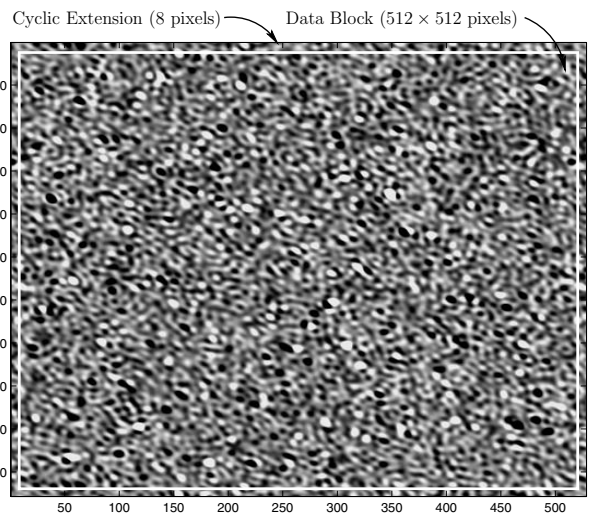


Fig. 4. A SDMT symbol with cyclic extension.

compress the dynamic range of the signal by nearly 30% using an iterative projection technique [27].

The transmitted image is formed by taking the inverse fast Fourier transform (IFFT) of the 512×512 pixel image. A *cyclic extension* is appended around the edges of the transmitted frame. The benefit of this extension is that the linear convolution of the channel response with the image is equivalent to a circular convolution and so equalization at the receiver is a matter of a single complex multiplication per bin. This cyclic extension is analogous to the cyclic prefix added in conventional DMT systems [25]. The transmitter clips and quantizes the transmitted signal to the 8-bit resolution of the transmit array. Fig. 4 illustrates a typical SDMT symbol with cyclic extension.

At the receiver, the received image is sampled in time and in space. It is assumed that the temporal synchronization is exact and that there is no temporal ISI present in the channel. Since no spatial filtering is available, aliasing is an impairment at the front end of the receiver. Although the transmitted signal can be designed with no energy beyond the Nyquist band, the clipping and quantization noise generated in the transmitter fold back into the Nyquist band. This aliased noise is considered in the power allocation in Sec. III-B. It is further assumed that the receiver has performed registration of the transmitter in its field-of-view. Spatial synchronization of the receiver to the transmitted image is eased since no inter-bin interference is present if the spatial frequency resolutions of the spatially sampled transmitted and receive images are adjusted to be the same. The received image is placed in frequency domain using a 154×154 point fast Fourier transform (FFT) and equalized using a single complex multiplication per spatial frequency bin.

B. Capacity Estimate

The experimental channel considered here is peak-limited and it is not clear how to represent this constraint directly in frequency domain. However, it is possible to model the

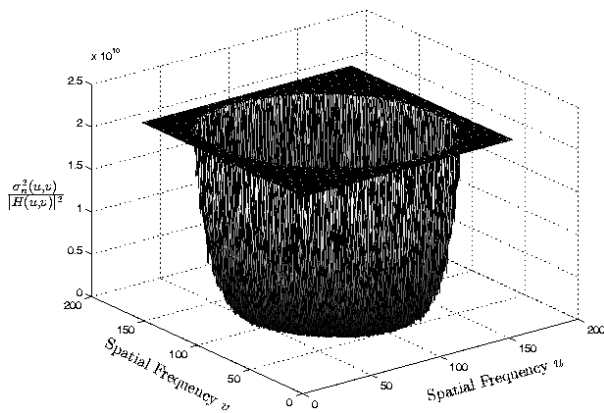


Fig. 5. Water-pouring “bowl” for the SDMT channel.

channel as a conventional electrical channel if an electrical power allocation is selected to minimize clipping distortion. Let E be a measure of the total electrical energy distributed among the frequency bins in the Nyquist band of the receiver. A limit on E can be estimated by bounding the maximum amplitude due to the four adjacent pixels. Simulations verify that over many symbols the resulting clipping distortion present in the output image is small and well modelled as a broadband spatial frequency noise source. In this design, the signal dependent characteristic of clipping and quantization noise sources is not considered directly. Rather, the noise spectrum per bin is estimated by running 50 frames through the channel model when the power allocation is set to spread E over all bins equally. The noise power received in each frequency bin within the Nyquist band of the receiver is then averaged to form an estimate of the noise spatial frequency distribution, $\sigma_n^2(u, v)$. Furthermore, we assume that the noise sources in each spatial frequency bin are independent Gaussian processes.

With an estimate of the noise variance in each bin, an electrical power allocation amongst the spatial frequency bins in the Nyquist band is derived using the well-known water-pouring spectrum [28]. Fig. 5 presents a plot of the water-pouring “bowl” for channel optical transfer function $H(u, v)$. The power allocation can be viewed as a process in which the constraint E is poured into the bowl and occupies those channels with the lowest $\sigma_n^2(u, v)/|H(u, v)|^2$. It should be noted that not all spatial frequency points in the Nyquist band of receiver have power allocated to them. The vertical axis in Fig. 5 is truncated to allow for plotting.

The capacity of the SDMT system can be estimated as the sum of a series of parallel Gaussian noise channels. Using the estimated noise variance per bin along with the computed power allocation the capacity of the channel is estimated to be 22.4 kbits/frame. This capacity does not explicitly take into account the peak constraint of the channel, but rather models the channel as an electrical channel with added Gaussian-distributed clipping noise.

C. Code Design

In order to approach the rates promised by the capacity estimate, we apply multi-level codes and multi-stage decoding over the spatial frequency bins. Let $B = (b_0, b_1, \dots, b_{M-1})$ be the address bits required for a 2^M point constellation. The mutual information from input to output can be written as,

$$I(Y; B) = \sum_{i=0}^{M-1} I(Y; b_i | b_{i-1}, b_{i-2}, \dots, b_0).$$

Thus, data transmission on this channel can then be viewed as communication on M parallel bit channels, b_i , assuming b_{i-1}, \dots, b_0 are known [29]. Multi-level codes assign a binary code, C_i , to each b_i depending on the “quality” of the given bit channel. If each C_i is capacity achieving, then the total channel capacity is achieved using multi-level coding and multi-stage decoding [29].

In the context of DMT channels, it has been found that the use of multi-level codes can approach the channel capacity over a wide class of channels [30]. For the SDMT channel described in Sec. III-B, multi-level codes are applied to approach the computed channel capacity. Following [30], the bit loading algorithm selects the smallest constellation, of size 2^i for $i = 1, \dots, 8$, for each frequency bin so that the rate loss is at most 0.2 bits/symbol. Bits b_0 and b_1 in each bin are Gray labelled and treated as a single symbol. Subject to the loading algorithm, the average capacity of $b_0 b_1$ over all the frequency bins was computed to be 0.56 bits/symbol. The intuition is that since there are a large number of bins a long, powerful code with rate near the average capacity of $b_0 b_1$ will perform well. These two bits in each spatial frequency bin are coded with a near capacity achieving, irregular rate-1/2 low density parity check code (LDPC) with block length 10^5 [30]. Simulations indicate that this code converges under the channel bin SNRs computed in Sec. III-B. At the decoder, the log-likelihood ratios for each of these bits can be computed over all constellation points and input to the LDPC decoder.

The higher level bits are labelled using Ungerboeck’s set partitioning labelling where for each bit the intra-set distance increases. In order to design codes for the upper bits, a target bit-error rate of 10^{-7} was set. The upper bit channels are modelled as binary symmetric channels (BSCs) and hard decision Reed-Solomon codes of block length 255 were applied to ensure that the target error rate was met. Table I presents the average conditional probability of error for the higher order bits along with the capacity of the associated BSCs. For b_5 and higher bits, uncoded transmission satisfies the error rate target.

After applying multi-level codes, the resulting rate over all frequency bins was computed to be 17.1 kbits/frame or 76% of the estimated channel capacity. The resulting spectral efficiency of the system is dependent on the pulse shape used for the underlying PAM modulation for each pixel. In this case, rectangular PAM modulation was employed for each pixel. Using a 99% fractional power definition of bandwidth the ultimate spectral efficiency achieved is 1.7 kbits/s/Hz.

TABLE I
CODE DESIGN FOR HIGHER LEVEL BIT LABELS.

Bit	$Pe(b_i b_0 \dots b_{i-1})$	Capacity of BSC	RS Code	Rate
b_2	0.01598	0.8818	(255,133)	0.5216
b_3	3.5258×10^{-4}	0.9954	(255,237)	0.9294
b_4	1.0371×10^{-6}	0.9999	(255,249)	0.9765
b_5	1.6014×10^{-11}	-	uncoded	-

The case of “pixel-matched” signalling was also considered using the same channel model. In this case images are formed by transmitting independent data on square blocks of pixels of size $K \times K$ and detecting each receive pixel independently. The maximum spectral efficiency over K can be shown to be less than 290 bits/s/Hz and is limited by inter-pixel interference caused by the low pass spatial frequency response [3].

The complexity of the required processing in a practical system, however, has not been taken into account as the goal of this work is to demonstrate the potential gains in spectral efficiencies afforded by the pixelated wireless optical channel.

IV. CONCLUSIONS AND FUTURE DIRECTIONS

The pixelated wireless optical channel provides large gains in spectral efficiency by leveraging the spatial diversity inherent to arrays of optical emitters and detectors. The increase in spectral efficiency is achieved through spatio-temporal coding which replaces the inefficient spatial repetition code of conventional multi-element wireless optical links.

Although spatially invariant channels are discussed here, SDMT may also be appropriate on channels with spatial variation. It is often the case in chip-to-chip optical signalling that the gain of pixels may vary across the array or even be zero. If the spatial variation was known *a priori* at the transmitter, say during a calibration stage in manufacture, it can be taken into account in the power allocation algorithm. It should also be noted that the pixelated transmitter and receiver need not be planar. Indeed, hemispherical or other shaped transmitters may be convenient in practical situations and relieve the orientation problem inherent to point-to-point links. Such non-planar transmitters can be fabricated using OLED panels. Additionally, practical pixelated links can also be implemented in the infrared band using proper transmitter and receiver arrays.

REFERENCES

[1] J. M. Kahn, W. J. Krause, and J. B. Carruthers, “Experimental characterization of non-directed indoor infrared channels,” *IEEE Trans. Commun.*, vol. 43, no. 2/3/4, pp. 1613–1623, Feb./Mar./Apr. 1995.

[2] J. M. Kahn and J. R. Barry, “Wireless infrared communications,” *Proc. IEEE*, vol. 85, no. 2, pp. 263–298, Feb. 1997.

[3] S. Hranilovic, *Spectrally Efficient Signalling for Wireless Optical Intensity Channels*, Ph.D. thesis, Dept. of Elec. & Comp. Engineering, University of Toronto, 2003.

[4] J. B. Carruthers and J. M. Kahn, “Angle diversity for nondirected wireless infrared communication,” *IEEE Trans. Commun.*, vol. 48, no. 6, pp. 960–969, June 2000.

[5] S. Jivkova and M. Kavehrad, “Receiver designs and channel characterization for multi-spot high-bit-rate wireless infrared communications,” *IEEE Trans. Commun.*, vol. 49, no. 12, pp. 2145–2153, Dec. 2001.

[6] G. Yun and M. Kavehrad, “Spot-diffusing and fly-eye receivers for indoor infrared wireless communications,” in *Proc. IEEE Int. Conf. Sel. Topics in Wireless Commun.*, 1992, pp. 262–265.

[7] P. Djahani and J. M. Kahn, “Analysis of infrared wireless links employing multibeam transmitters and imaging diversity receivers,” *IEEE Trans. Commun.*, vol. 48, no. 12, pp. 2077–2088, Dec. 2000.

[8] J. M. Kahn, R. You, P. Djahani, A. G. Weisbin, B. K. Teik, and A. Tang, “Imaging diversity receivers for high-speed infrared wireless communication,” *IEEE Commun. Mag.*, vol. 36, no. 12, pp. 88–94, Dec. 1998.

[9] K. Akhavan, M. Kavehrad, and S. Jivkova, “High-speed power-efficient indoor wireless infrared communication using code combining – Part I,” *IEEE Trans. Commun.*, vol. 50, no. 7, pp. 1098–1109, July 2002.

[10] K. Akhavan, M. Kavehrad, and S. Jivkova, “High-speed power-efficient indoor wireless infrared communication using code combining – Part II,” *IEEE Trans. Commun.*, vol. 50, no. 9, pp. 1495–1502, Sept. 2002.

[11] D. V. Plant, M. B. Venditti, E. Laprise, J. Faucher, K. Razavi, M. Châteauneuf, A. G. Kirk, and J. S. Ahearn, “256-channel bidirectional optical interconnect using VCSELs and photodiodes on cmos,” *IEEE J. Lightwave Tech.*, vol. 19, no. 8, pp. 1093–1103, Aug. 2001.

[12] M. Châteauneuf, A. G. Kirk, D. V. Plant, T. Yamamoto, and J. D. Ahearn, “512-channel vertical-cavity surface-emitting laser based free-space optical link,” *IEEE J. Lightwave Tech.*, vol. 41, no. 26, pp. 5552–5561, Sept. 2002.

[13] D. V. Plant and A. G. Kirk, “Optical interconnects at the chip and board level: Challenges and solutions,” *Proc. IEEE*, vol. 88, no. 6, pp. 806–818, June 2000.

[14] M. A. Neifeld and R. K. Kostuk, “Error correction for free-space optical interconnects: Space-time resource optimization,” *Optics Lett.*, vol. 37, no. 2, pp. 296–307, Jan. 1998.

[15] T. H. Szymanski, “Bandwidth optimization of optical data link by use of error-control codes,” *Optics Lett.*, vol. 39, no. 11, pp. 1761–1775, Apr. 2000.

[16] J. Faucher, M. B. Venditti, and D. V. Plant, “Application of parallel forward-error correction in two-dimensional optical-data links,” *IEEE J. Lightwave Tech.*, vol. 21, no. 2, pp. 466–475, Feb. 2003.

[17] R. M. Shelby, J. A. Hoffnagle, G. W. Burr, C. M. Jefferson, M.-P. Bernal, H. Coufal, R. K. Grygier, H. Günther, R. M. Macfarlane, and G. T. Sincerbox, “Pixel-matched holographic data storage with megabit pages,” *Optics Lett.*, vol. 22, no. 19, pp. 1509–1511, Oct. 1997.

[18] G. W. Burr, J. Ashley, H. Coufal, R. K. Grygier, J. A. Hoffnagle, C. Michael Jefferson, and B. Marcus, “Modulation coding for pixel-matched holographic data storage,” *Optics Lett.*, vol. 22, no. 9, pp. 639–641, May 1997.

[19] B. G. Boone, *Signal Processing Using Optics: Fundamentals, Devices, Architectures, and Applications*, Oxford University Press, New York, NY, 1998.

[20] NEC Solutions America, NEC Versa Web Site, support.neccomp.com/hardware/notebooks/versa6000/.

[21] Basler Vision Technologies, Web Site, www.basler-vc.com.

[22] R. Klette, K. Schlüns, and A. Koschan, *Computer Vision: Three-Dimensional Data from Images*, Springer-Verlag, Singapore, 1998.

[23] G. C. Holst, *CCD Arrays, Cameras, and Displays*, SPIE Optical Engineering Press, Bellingham, WA, 1996.

[24] J. M. Cioffi, “Asymmetric digital subscriber lines,” in *Communications Handbook*, J. D. Gibson, Ed., chapter 34, pp. 450–479. CRC Press / IEEE Press, Boca Raton, FL, 1997.

[25] J. S. Chow, J. C. Tu, and J. M. Cioffi, “A discrete multitone transceiver system for HDSL applications,” *IEEE J. Select Areas in Commun.*, vol. 9, no. 6, pp. 895–908, Aug. 1991.

[26] J. A. C. Bingham, “Multicarrier modulation for data transmission: An idea whose time has come,” *IEEE Commun. Mag.*, pp. 5–14, May 1990.

[27] A. Gatherer and M. Polley, “Controlling clipping probability in DMT transmission,” in *31st Asilomar Conference on Signals, Systems & Computers*, 1997, vol. 1, pp. 578–584.

[28] T. M. Cover and J. A. Thomas, *Elements of Information Theory*, Wiley & Sons Publishers, New York, NY, 1991.

[29] U. Wachsmann, R. F. H. Fischer, and J. B. Huber, “Multilevel codes: Theoretical concepts and practical design rules,” *IEEE Trans. Inform. Theory*, vol. 45, no. 5, pp. 1361–1391, July 1999.

[30] M. Ardakani, T. Esmailian, and F. R. Kschischang, “Near-capacity coding in multi-carrier modulation systems,” *IEEE Trans. Commun.*, submitted for publication.